Photoacoustics 25 (2022) 100318

Contents lists available at ScienceDirect

Photoacoustics

journal homepage: www.elsevier.com/locate/pacs

Compact and portable quartz-enhanced photoacoustic spectroscopy sensor for carbon monoxide environmental monitoring in urban areas

Fabrizio Sgobba [a], Angelo Sampaolo [a,b], Pietro Patimisco [a,b], Marilena Giglio [a], Giansergio Menduni [a], Ada Cristina Ranieri [a,c], Christine Hoelzl [d], Hubert Rossmadl [d], Christian Brehm [d], Verena Mackowiak [d], Dario Assante [c], Ezio Ranieri [e], Vincenzo Spagnolo [a,b,*]

[a] PolySense Lab, Dipartimento Interateneo di Fisica, University and Politecnico of Bari, CNR-IFN, Via Amendola 173, Bari 70126 Italy
[b] PolySense Innovations srl, Via Amendola 173, Bari 70126 Italy
[c] Faculty of Engineering, Uninettuno University, 00186 Rome, Italy
[d] Thorlabs GmbH, Münchner Weg 1, 85232 Bergkirchen, Germany
[e] Biology Department, University of Bari, Via Orabona 4, 70126 Bari, Italy

ARTICLE INFO

Keywords:
Quartz enhanced photoacoustic spectroscopy
Gas sensing
Carbon monoxide
Environmental monitoring
Energy relaxation processes

ABSTRACT

We report on the realization, calibration, and test outdoor of a 19-inches rack 3-units sized Quartz Enhanced Photoacoustic Spectroscopy (QEPAS) trace gas sensor designed for real-time carbon monoxide monitoring in ambient air. Since CO acts as a slow energy relaxer when excited in the mid-infrared spectral region, its QEPAS signal is affected by the presence of relaxation promoters, such as water vapor, or quenchers like molecular oxygen. We analyzed in detail all the CO relaxation processes with typical collisional partners in an ambient air matrix and used this information to evaluate oxygen and humidity-related effects, allowing the real CO concentration to be retrieved. The sensor was tested outdoor in a trafficked urban area for several hours providing results comparable with the daily averages reported by the local air inspection agency, with spikes in CO concentration correlated to the passages of heavy-duty vehicles.

1. Introduction

Among all the environmental pollutants, carbon monoxide (CO) is by far one of the most dangerous and most common compounds. Its colorless, odorless, tasteless and flammable nature and its ready reaction with hemoglobin to form carboxyhemoglobin makes this compound extremely toxic for humans and animals. CO is produced in the incomplete combustion of carbon-containing fuels, such as gasoline, natural gas, oil, coal, and wood. Motor-vehicle emissions are the primary source of CO in outdoor air in urban areas. High concentrations of CO lead to reduced oxygen transport by hemoglobin, with health effects that include headaches, increased risk of chest pain for persons with heart disease. CO is also one of the main causes of unintentional as well as suicidal poisoning, causing annually many deaths from hypoxia. The World Health Organization (WHO) traced specific guidelines regarding maximum suggested exposure time for different CO concentrations in air (chapter 5, Section 5 in [1]), as reported in Table 1.

CO background concentration in troposphere in non-urban, unpolluted areas usually spans in the $\sim 0.05-0.3$ parts-per-million (ppm) range [2],[3], as recently confirmed by the data collected in the Measurements of Pollution in the Troposphere (MOPITT) NASA mission [4]. Nevertheless, these values may grow up to $1-25$ ppm in urban or metropolitan areas because of vehicles exhaust or industrial emissions [5,6]. In closed environments (such as houses or offices), carbon monoxide may reach the worrying concentrations of $150-3000$ ppm due to indoor fires, depending on ventilation condition of the room [7]. Therefore, carbon monoxide-related pollution represents a major threat for air quality (both outdoor and indoor) and public safety and the detection of leakages and emissions of such highly toxic pollutant turns out as a substantial challenge for almost any actor in the heavy, chemical, automotive and oil and gas industry.

In this paper, we present a CO sensor based on Quartz-Enhanced Photoacoustic Spectroscopy (QEPAS). This technique consists in exciting the target gas molecules with a modulated laser light. In the

Abbreviations: QEPAS, Quartz-Enhanced PhotoAcoustic Spectroscopy.

* Corresponding author at: PolySense Lab, Dipartimento Interateneo di Fisica, University and Politecnico of Bari, CNR-IFN, Via Amendola 173, Bari 70126, Italy.
E-mail address: vincenzoluigi.spagnolo@poliba.it (V. Spagnolo).

https://doi.org/10.1016/j.pacs.2021.100318
Received 28 September 2021; Received in revised form 9 November 2021; Accepted 22 November 2021
Available online 25 November 2021

Table 1
WHO guidelines for CO exposure.

Concentration	Maximum exposure time
90 parts per million (ppm)	15 min
50 ppm	30 min
25 ppm	1 h
10 ppm	8 h

mid-IR spectral range, at the usually employed working pressures (ranging between a few hundred Torr and atmospheric pressure), excited molecules relaxation through spontaneous emission is sufficiently slow (ms timescale) to be entirely neglected [8,9]. This means that the molecules relaxation from the excited state to the fundamental state occurs almost exclusively via nonradiative relaxation, i.e., rotational to translational (R-T), vibrational to vibrational (V-V) and vibrational to translational (V-T) collisions with the surrounding molecules composing the mixture. Such an energy release causes a local increase of the gas temperature and, therefore, of the gas pressure. Since the laser is modulated, pressure waves, i.e., sound waves, are generated, further detected employing a quartz tuning fork (QTF) as a sound-to-current transducers, due to the quartz piezoelectric properties [9–11]. QEPAS, along with other QTF-based techniques, has been already demonstrated to be capable to perform CO real time detection in the sub-ppm range [8,12–15] or even in the ppt range [16]. However, CO is a slow relaxer for the typical QTF operating frequencies ($10 - 32.8kHz$) and the QEPAS signal is strongly affected by the presence of relaxation promoters in the mixture. The dependence of CO mid-IR QEPAS signal from water vapor has been investigated in [12,13] and both theoretically predicted and experimentally analyzed in [8]. Nevertheless, an extensive theoretical and experimental investigation on CO relaxation in humid and dry air and its effect on QEPAS signal is still missing and this represents an essential step toward CO detection in ambient air for real word applications.

Starting from the study presented in [8], a modeling of CO relaxation in airlike humidified gas matrices has been developed in this paper. A compact and portable QEPAS-based CO sensor tailored for outdoor real time monitoring has been designed, realized and tested under different humidity and diluting gas conditions. The sensor prototype has been tested nearby a traffic light in an urban area for several hours to demonstrate the proposed sensor as a reliable ambient real-time CO detector.

2. Prototype sensor design

In Fig. 1a the architecture of the carbon monoxide QEPAS-based 19-inches rack 3-units sized sensor, is reported. A picture of the realized prototype is also shown in Fig. 1b. An AdTech High Heat Load (HHL)-packaged Distributed Feedback (DFB) - Quantum Cascade Laser (QCL) emitting at $\sim 4.57\mu m$ has been employed as the exciting laser source targeting the CO absorption line located at $2190.02cm^{-1}$. This line corresponds to the R-12th branch of the fundamental ($\Delta\tilde{\nu} = 1$) vibrational transition of the carbon monoxide with a line-strength of $2.9 \times 10^{-19} cm/mol$ [17]. The selected line was targeted by operating the QCL at 18°C and an injection current of $246.3mA$, with an optical power of $32.3mW$. The QCL collimated output beam was focused by an anti-reflection coated 40 mm-focal CaF_2 lens between the prongs of the QTF, inside the acoustic detection module (ADM). The ADM employed in this prototype implemented a spectrophone composed of a T-Shaped QTF having resonance frequency of $f_0 = 12.47kHz$ (QTF S08-T in [18]) and a couple of micro-resonator tubes (12.4 mm long and 1.59 mm internal diameter) in on-beam configuration, to amplify the sound waves. This specific spectrophone geometry was demonstrated to achieve the best performances in terms of signal to noise ratio (SNR) [19,20] and QEPAS signal (SP2 in [18]). More than 98% of optical power passes through the spectrophone. The ADM included also two BaF_2 wedged windows anti-reflection coated. The 2f-detection wavelength modulation (WM) QEPAS technique was implemented by modulating the laser current with a frequency of $f_0/2$ and acquiring the f_0-oscillating component of the spectrophone signal output.

Pressure and flow inside the ADM are set and continuously monitored by means of a pressure controller and a flow, as schematically shown in Fig. 1a. The ADM employed in this prototype has been equipped with a miniaturized pressure-temperature-humidity (PTH) meter to measure continuously the water vapor concentration in the mixture.

The electronics employed for the prototype consists of different boards (see Fig. 1a), to drive and modulate the HHL QCL, keeps its temperature stable, and acquire and demodulate the QTF signal. A LabVIEW-based software has been developed to run the 19-inches rack 3-units sized sensor prototype (Fig. 1b) remotely and perform both QTF electrical characterization and QEPAS measurements (either at fixed or scanning wavelength), while continuously measuring pressure, humidity, and flow inside the ADM.

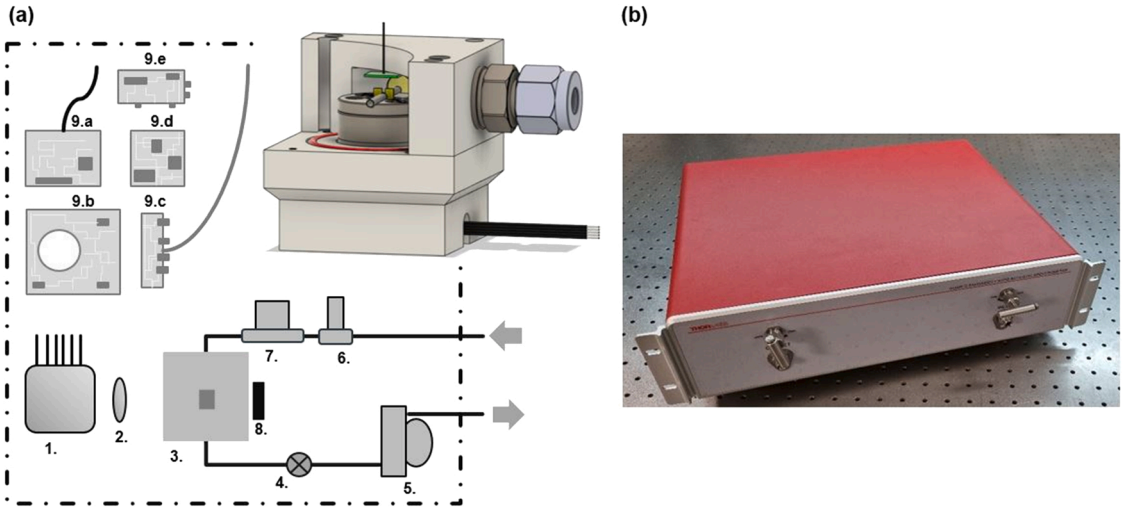

Fig. 1. (a) Schematic of the prototype architecture. 1. HHL DFB-QCL; 2. Lens; 3. Acoustic detection module (also depicted in 3D, top right corner); 4. Needle valve; 5. Pump; 6. Pressure controller; 7. Flow meter; 8. Power meter for optical alignment; 9. Electronics. Arrows indicate gas flow direction. (b) Photo of the realized 19-inches rack 3-units sized CO sensor. Length x Width x Height = 36 cm x 48,2 cm x 13,3 cm; weight = 10 Kg.

3. A theoretical model for carbon monoxide mid-IR relaxation

3.1. Pure N_2 as the diluting gas

The targeted absorption line, falling at $2190.02cm^{-1}$, represents the transition described by the couple of quantic numbers $(\tilde{v}, J)$: $i = (0,12) \rightarrow f = (1,13)$ [8,17]. In the mid-IR, considering the pressures of interest for photo-acoustic spectroscopy (PAS), usually ranging between a few hundred Torr and atmospheric pressure, excited molecules relaxation through spontaneous emission is sufficiently slow (ms timescale) to be entirely neglected [8,9]. This means that the CO relaxation from the excited state f to the fundamental state $(0,0)$ occurs almost exclusively via nonradiative relaxation, i.e., rotational to translational (R-T), vibrational to vibrational (V-V) and vibrational to translational (V-T) collisions with the surrounding molecules composing the mixture. Considering as a first instance CO diluted in dry N_2, for low CO concentrations (below 100 ppm), the V-T relaxation of CO onto a CO energy level can be neglected, as well as any vibrational back transfer N_2-CO. Thereby, the fastest relaxation path for CO is constituted by the V-V collision with N_2, having a rate of $\gamma^{VV}_{CO-N2} \approx 1.4 \times 10^5 s^{-1} atm^{-1}$ [10]. The energy level of N_2 ($2331cm^{-1}$) is located above the CO first vibrational overtone ($2145cm^{-1}$), giving rise to an endothermic process. If the mixture is humidified, a new exothermic relaxation path V-$V_{CO\text{-}H2O}$ becomes available, corresponding to an energy level of 1595 cm^{-1} and a rate of $\gamma^{VV}_{CO-H2O} \approx 5.5 \times 10^6 s^{-1} atm^{-1}$ [10]. These two processes are therefore in competition, and the CO QEPAS signal vs H_2O concentration inside the mixture first drops down to a minimum (representing a progressive averaging of the two contributions) and then progressively increases (meaning that water relaxation promotion starts dominating).

Because of their extremely fast roto-translational relaxation ($\gamma^{RT}_{CO-N2} \approx 2.3 \times 10^9 s^{-1} atm^{-1}$ [8]) it is possible to assume that the CO molecules are excited directly to the rotational thermal equilibrium of the excited vibrational mode. Such an assumption simplifies the rate equations, which now involve only vibrational energy transfer. The simplified system can be described with following set of equations [8]:

$$\frac{dN_{CO^*}}{dt} = \Phi(t) - N_{CO^*}\left(\gamma^{VV}_{CO-N2} \cdot \wp_{N2} + \gamma^{VV}_{CO-H2O} \cdot \wp_{H2O}\right) \quad (1)$$

$$\frac{dN_{N2^*}}{dt} = N_{CO^*} \cdot \gamma^{VV}_{CO-N2} \cdot \wp_{N2} - N_{N2^*}\left(\gamma^{VT}_{N2} \cdot \wp_{N2} + \gamma^{VT}_{N2-H2O} \cdot \wp_{H2O}\right) \quad (2)$$

$$\frac{dN_{H2O^*}}{dt} = N_{CO^*} \cdot \gamma^{VV}_{CO-H2O} \cdot \wp_{H2O} + N_{N2^*} \cdot \gamma^{VV}_{N2-H2O} \cdot \wp_{H2O} - N_{H2O^*}\left(\gamma^{VT}_{H2O-N2} \cdot \wp_{N2} + \gamma^{VT}_{H2O} \cdot \wp_{H2O}\right) \quad (3)$$

Where N_{M^*} is the population density function in the excited level of a specific molecule M, $\wp_M$ is its partial pressure (total pressure is assumed to be the optimal one, $P = 500Torr$) inside the mixture and γ^{VT}_M and $\gamma^{VV}_{M-M'}$ are the relaxation rates for V-T and V-V collisions respectively. The γ parameters are summarized in Table 2.

In Eq. (1), $\Phi(t)$ represents the pump term related to the photon absorption, and results:

$$\Phi(t) = N_{COi} \frac{A_{21}}{8\pi h \nu(t)^3} \frac{g_f}{g_i} \Gamma(\nu(t)) \frac{I(t)}{c^2} \quad (4)$$

Where A_{21} is the Einstein's A coefficient, $\nu(t)$ is the emission wavenumber (varied sinusoidally in frequency modulation technique), $g_f/g_i = (2J_f + 1)/(2J_i + 1)$ [25] is the gyroscopic ratio between the initial and the final state, $\Gamma(\nu(t))$ is the profile of the absorption feature at the chosen working pressure, $I(t)$ is the laser intensity and c is the speed of light. N_{COi} represents the number of CO molecules effectively allowed to absorb the photon, occupying the initial energy-angular momentum state i.

In typical QEPAS operating pressures, R-T relaxation time is in the $\tau_{RT} \approx 0.1 - 0.01ns$ timescale, which is 5–6 orders of magnitude smaller than laser modulation period ($\tau_{laser} \approx 0.16ms$ in our experiments). R-T recombination can therefore be assumed as instantaneous, which together with the low optical power involved leads to the following approximations during N_{COi} evaluation:

- Depletion of the ith state can be neglected.
- fth state is far from population inversion condition and any bleaching effect due to absorption can be neglected.

Under these assumptions, N_{COi} can be calculated as [25]:

$$N_{COi} = \frac{g_i N_{CO}}{G_{TOT}(T)} e^{-\frac{E_i}{k_B T}} \quad (5)$$

Where N_{CO} is the total number per unit volume of CO molecules in the mixture, $G_{TOT}(T)$ is the total partition sum of the CO gas at the chosen temperature T and $E_i = hc\mathscr{B}J_i^2$, with $\mathscr{B}$ the rotational constant ($\mathscr{B} = 1.9cm^{-1}$ for $^{12}C^{16}O$), E_i is the energy associated to the i-th level.

The assumption to neglect any radiative emission (spontaneous as well as stimulated) in this range allows to evaluate the thermal energy dissipated per unit volume and time, $\mathscr{K}(t)$, as the sum of all nonradiative relaxation contributions (here indexed with r) [8,21,22]:

$$\mathscr{K}(t) = \sum_{M,M',r} \left(hc\nu_r N_{M^*}(t) \gamma^r_{M-M'} \wp_{M'}\right) + hc\nu_{RT} \gamma^{RT}_{CO-N_2} \Phi(t) \wp_{N_2} \quad (6)$$

The process of heating of the gas sample via CO relaxation results to be isochoric due to the boundary constraints imposed by the metallic walls. Moreover, in low gas flow regime (tens of standard cm^3) any mass exchange happens in timescales several orders of magnitude greater than modulation period τ_{laser}, and the gas can therefore be considered as isolated, as far as concerns the PAS process. Thereby, it is possible to combine the first law of thermodynamics in isochoric conditions with the ideal gas law:

$$\mathscr{K} = \Delta U = C_V \Delta T = \frac{C_V}{Rn} \Delta P = \frac{1}{\gamma - 1} \Delta P \quad (7)$$

Table 2
Rate intensity of the different V-V and V-T relaxations channels involving CO, N_2 and H_2O.

Process involved	Rate intensity ($s^{-1}atm^{-1}$)	Reference in literature
$CO^* + N_2 \rightarrow CO + N_2^*$,	1.4×10^5	[8]
$CO^* + H_2O \rightarrow CO + H_2O^*$, γ^{VV}_{CO-H2O}	5.5×10^6	[8]
$N_2^* + H_2O \rightarrow N_2 + H_2O^*$, γ^{VV}_{N2-H2O}	2.2×10^5	[8,21–24]
$N_2^* + N_2 \rightarrow N_2 + N_2$, γ^{VT}_{N2}	1.7	[8,21,22]
$H_2O^* + H_2O \rightarrow H_2O + H_2O$, γ^{VT}_{H2O}	1.1×10^9	[10,19–22]
$H_2O^* + N_2 \rightarrow H_2O + N_2$, γ^{VT}_{H2O-N2}	1.2×10^7	[8,21–24]

Where Cv is the specific heat at constant volume, R is the gas constant, n is the number of moles. This leads to the conclusion that $\mathscr{H}(t)$ is converted into a variation in pressure P with a conversion factor $1/\gamma - 1$, where γ is the heat capacity ratio (for a diatomic gas at ambient temperature, $\gamma = 1.4$). In frequency modulation technique, both optical power and emission wavenumber of the laser are modulated as follows [8,9,26,27]:

$$\nu(t) = \nu_0 + \Delta\nu \quad cos\left(2\pi\frac{f_{QTF}}{2}t\right) \tag{8}$$

$$I(t) = I_0 + \Delta I \quad cos\left(2\pi\frac{f_{QTF}}{2}t\right) \tag{9}$$

In pressure regimes where pressure broadening of the absorption line dominates over Doppler broadening, the best frequency modulation depth is fixed by the relation $\Delta\nu \approx 1.1w$ [27], where w is the FWHM of the targeted absorption line at the working pressure. This constraint in the choice of modulation depth results in a negligible intensity depth ($\Delta I \approx 0$).

$\mathscr{H}(t)$ is a linear combination of the $N_{M^*}(t)$, solutions of a system of ordinary differential equations (ODE) having a pump term sinusoidally modulated with frequency $f_0/2$, which means $\mathscr{H}(t)$ can be written in terms of a Fourier series:

$$\mathscr{H}(t) = \sum_n \mathscr{H}_n(t) = \sum_n \mathscr{H}_n Exp\left(i2\pi n\frac{f_{QTF}}{2}t\right) \tag{10}$$

According to Eq. (7), localized and modulated heat production is converted into a pressure wave (or sound wave) which has $\mathscr{H}(t)$ itself as the source term and is the solution of the wave equation:

$$\frac{\partial^2}{\partial t^2}P - v^2\nabla^2 P = (\gamma - 1)\frac{\partial \mathscr{H}}{\partial t} \tag{11}$$

Where v is the speed of sound in air. Since the Fourier transform operation is linear, it is possible to write Eq. (11) for each one of the $\mathscr{H}_n(t)$ Fourier components described in Eq. (10), obtaining n pressure wave solutions $P_n(t)$. Since the QTF acts at the same time as a sharp frequency filter and as an acoustic wave detector, the only component extracted and amplified, when the wavelength modulation and $2f$ detection approach is employed, will be $P_2(t)$. In conclusion, the QEPAS signal results to be $S_{CO} \propto \mathscr{H}_2$.

A Python-based script has been written to solve iteratively the rate equations Eqs. (1–3) and calculate $\mathscr{H}_2$ varying the humidity conditions, while keeping fixed the CO concentration. $\mathscr{H}_2$ value, rescaled on the dry value, has been plotted for each water vapor concentration C_W in the 0 −1.55% range as reported in Fig. 2.

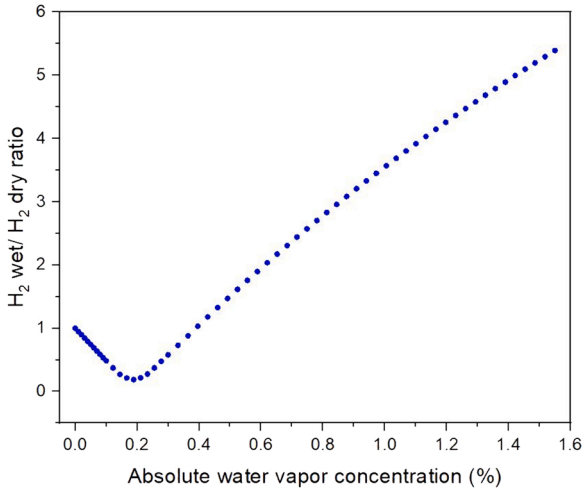

Fig. 2. Theoretical prediction of $\mathscr{H}_2$ value calculated for different water vapor concentrations and divided by the dry $\mathscr{H}_2$ value, plot obtained using a Python script.

The theoretical calculations confirm the qualitative behavior expected. The predicted minimum is located at $C_W = 0.191\%$, in agreement with the theoretical and experimental results reported in [8]. For water vapor concentrations lower than C_w the endothermic path (through N_2) dominates, whereas at higher concentrations range the exothermic path (through H_2O) dominates. Thermal energy ratio at its minimum results to be $\mathscr{H}_2(0.191\%)/\mathscr{H}_2(0) = 0.19$, whereas at the highest water concentration level is $\mathscr{H}_2(1.55\%)/\mathscr{H}_2(0) = 5.39$. In the concentration range of interest for this manuscript the dissipated thermal energy ratio turns out to be independent on the CO concentration.

3.2. Synthetic air as the diluting gas

The theoretical model proposed for CO relaxation in N_2 has to be modified, when O_2 is included to the mixture to mimic the experimental condition in "standard air", in which the sensor is planned to operate. In terms of simulation, standard synthetic air ($21\%O_2 : 79\%N_2$) replaced pure N_2 as the diluting gas. The introduction of O_2 in the mixture, and therefore the availability of a new molecular level ($1556cm^{-1}$), unlocks several other collisional processes, excluding CO* +O2→CO+O2 transitions since the probability of CO V-T collisions with other molecules, except the ones involving N_2 and H_2O, is much lower with respect to other possible relaxation paths [28]. The relaxation rates involving O_2 are summarized in Table 3:

Consequently, the rate Eqs. (1–3) have been modified considering oxygen contribution as:

$$\frac{dN_{CO^*}}{dt} = \Phi(t) - N_{CO^*}\left(\gamma^{VV}_{CO-N2}\bullet\wp_{N2} + \gamma^{VV}_{CO-H2O}\bullet\wp_{H2O} + \gamma^{VV}_{CO-O2}\wp_{O2}\right) \tag{12}$$

$$\frac{dN_{N2^*}}{dt} = N_{CO^*}\bullet\gamma^{VV}_{CO-N2}\bullet\wp_{N2} - N_{N2^*}\left(\gamma^{VV}_{N2-O2}\bullet\wp_{O2} + \gamma^{VT}_{N2-O2}\bullet\wp_{O2} + \gamma^{VT}_{N2}\bullet\wp_{N2} + \gamma^{VT}_{N2-H2O}\bullet\wp_{H2O}\right) \tag{13}$$

$$\frac{dN_{O2^*}}{dt} = N_{H2O^*}\bullet\gamma^{VV}_{H2O-O2}\bullet\wp_{O2} + N_{N2^*}\bullet\gamma^{VV}_{N2-O2}\bullet\wp_{O2} - N_{O2^*}\left(\gamma^{VV}_{O2-H2O}\bullet\wp_{H2O} + \gamma^{VT}_{O2}\bullet\wp_{O2} + \gamma^{VT}_{O2-N2}\bullet\wp_{N2} + \gamma^{VT}_{O2-H2O}\bullet\wp_{H2O}\right) \tag{14}$$

$$\frac{dN_{H2O^*}}{dt} = N_{CO^*}\bullet\gamma^{VV}_{CO-H2O}\bullet\wp_{H2O} + N_{N2^*}\bullet\gamma^{VV}_{N2-H2O}\bullet\wp_{H2O} + N_{O2^*}\bullet\gamma^{VV}_{O2-H2O}\bullet\wp_{H2O} - N_{H2O^*}\left(\gamma^{VT}_{H2O-N2}\bullet\wp_{N2} + \gamma^{VT}_{H2O-O2}\bullet\wp_{O2} + \gamma^{VT}_{H2O}\bullet\wp_{H2O}\right) \tag{15}$$

Eqs. (12–15) give a new $\mathscr{H}^*(t)$, and therefore a new $\mathscr{H}_2{}^*$ typical of airlike gas matrices.

To our knowledge, there are no data available from literature on the relaxation rate γ^{VV}_{CO-O2} related to the V-V collision $CO^* + O_2 \rightarrow CO + O_2{}^*$, and thus, to evaluate $\mathscr{H}_2{}^*(C_W)$ function in synthetic air information on this parameter has to be retrieved experimentally. Nonetheless, it is possible to predict $\mathscr{H}_2{}^*(C_W)$ behavior at least qualitatively:

Table 3
Rate intensity of the V-V and V-T relaxations involving O_2.

Process involved	Rate intensity ($s^{-1}atm^{-1}$)	Reference in literature
$O_2{}^* + H_2O \rightarrow O_2 + H_2O^*$, γ^{VV}_{O2-H2O}	1.3×10^6	[21,29]
$H_2O^* + O_2 \rightarrow H_2O + O_2{}^*$, γ^{VV}_{H2O-O2}	4.6×10^7	[30]
$N_2{}^* + O_2 \rightarrow N_2 + O_2{}^*$, γ^{VV}_{N2-O2}	1.5×10^2	[30]
$O_2{}^* + O_2 \rightarrow O_2 + O_2$, γ^{VT}_{O2}	6.4×10^1	[30]
$O_2{}^* + N_2 \rightarrow O_2 + N_2$, γ^{VT}_{O2-N2}	4.0×10^1	[21,29]
$N_2{}^* + O_2 \rightarrow N_2 + O_2$, γ^{VT}_{N2-O2}	1.0	[30]
$H_2O^* + O_2 \rightarrow H_2O + O_2$, γ^{VT}_{H2O-O2}	6.0×10^4	[30]
$O_2{}^* + H_2O \rightarrow O_2 + H_2O$, γ^{VT}_{O2-H2O}	1.1×10^6	[22]

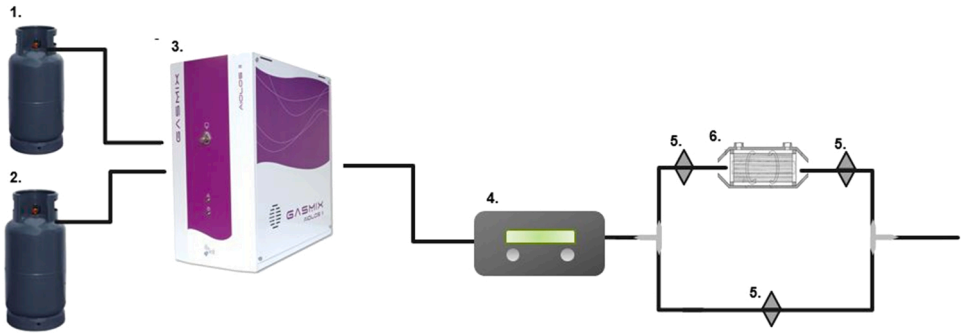

Fig. 3. Schematic of the gas handling system: 1. Diluting gas bottle; 2. Test gas bottle; 3. Gas mixer; 4. flow regulation electronic device (FReD); 5. On/off valves; 6. Permselect humidification membrane.

a) $\gamma_{CO-O2}^{VV} \approx \gamma_{CO-N2}^{VV}$ $\mathscr{H}_2^*(C_W)$ will display a linear behavior, with a negligible intercept (dry signal is expected to be close to zero).
b) $\gamma_{CO-O2}^{VV} \gg \gamma_{CO-N2}^{VV}$ Exothermic process is dominant even for low water concentrations. There is no minimum in the $\mathscr{H}_2^*(C_W)$ function.
c) $\gamma_{CO-O2}^{VV} \ll \gamma_{CO-N2}^{VV}$ The $\mathscr{H}_2^*(C_W)$ will resemble the $\mathscr{H}_2(C_W)$ obtained for a diluting gas of pure N_2.

With the aim of monitoring and measuring CO signal at different humidity and CO concentrations, a specifically tailored gas handling system has been built (see Fig. 3) and connected to the prototype gas-in connector.

4. Experimental procedure and results

The cylinders containing the certified mixture CO:N_2 and diluting gas were connected to a gas mixing system, composed of a gas mixer and a flow regulation electronic device (FReD), designed to produce flow-controlled dilutions. A humidification system was connected downstream with respect to the FReD. It consisted of two gas lines assembled by using two T-shaped connectors, the first one, the "wetting" line, is equipped with a PermSelect membrane filled with distilled water and placed between two on-off valves, while the second "dry" line is equipped with a single on-off valve.

The humidification and de-humidification processes were carried out using the following procedure: once the chosen CO concentration was selected from the gas mixer, only the dry line was opened. After a few minutes, the dry line was closed and the humidified one opened. The mixture humidity level was then monitored via software, by reading the data coming from the PTH inside the ADM. Once the mixture was saturated, reaching a saturation value of ~1.55% water vapor concentration (process that took usually no more than 30–45 min), the valves were suddenly switched to the initial position, closing the humidified line and opening the dry one. The measurements taken varying humidity were performed only in this third step, following the continuous and slow drop in water concentration (which by contrast took several hours). The flow was simultaneously monitored upstream (FReD) and downstream (flow meter) with respect to the humidification line, to ensure and monitor the line seal.

Preliminary investigations allowed to identify the optimal operating conditions in terms of gas sample pressure and flow, and QCL amplitude modulation. All the measurements presented in this paper were performed at a pressure of 500 Torr and by modulating the laser current with an amplitude of 290 mV_{pp}.

4.1. Sensor calibration

The sensor calibration was performed in controlled humidity conditions, by setting the water vapor content up to the saturation value of $C_W = 1.55\%$, well above the reading threshold value of the employed PTH sensor $C_{Wb} = 0.125\%$.CO concentration inside the humidified line was varied by mixing 9.82*ppm CO:*N_2 with pure N_2 down to 50 parts-per-billion (ppb). For each CO concentration value, a spectral scan around the peak, taken at 1*s* integration time, was performed. A selection of measured spectra is shown in Fig. 4a. Every peak value was

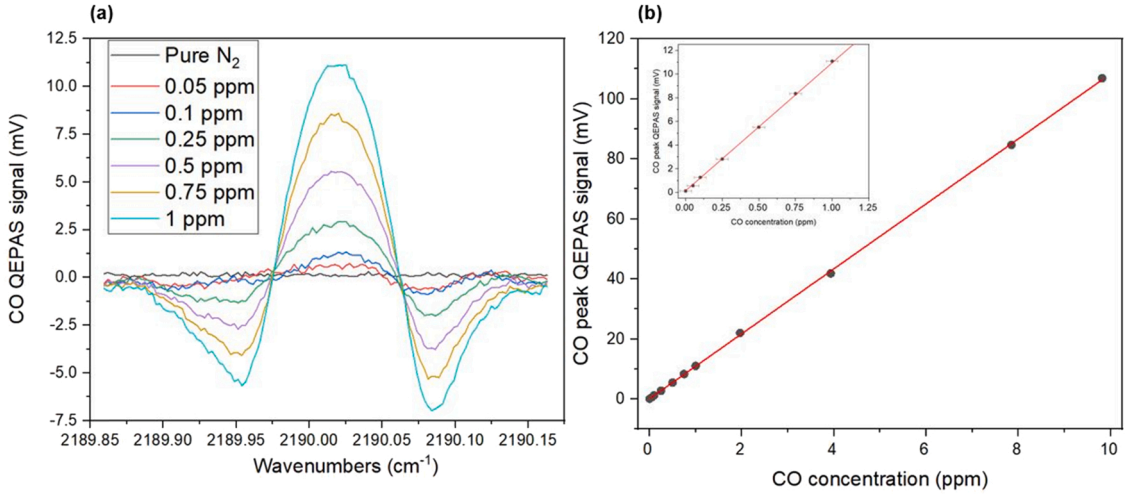

Fig. 4. a): Spectral scan of CO absorption line at different CO concentrations, while keeping the water concentration fixed at $C_W = 1.55\%$. b): peak signal value plotted as a function of CO concentration (black dots) and the related best linear fit (red line). In the inset is shown an expanded view of the linear fit in the ppb range of concentrations.

extracted, plotted as a function of the CO concentration and the results linearly fitted, as reported in Fig. 4b.

The CO QEPAS peak signal displays a linear trend ($R^2 \approx 0.9998$) versus concentration in the whole analyzed concentration range. The fit provided the following calibration curve:

$$S_{CO,sat} = 10.82\frac{mV}{ppm}C_{CO}(ppm) + 0.11mV \quad (16)$$

The intercept is comparable with the noise level $\sigma = 0.11mV$ evaluated in pure N_2.

4.2. Water vapor-promoted CO relaxation in pure N_2

Once the QEPAS peak calibration in saturated mixture was completed, the subsequent step consisted in the investigation of QEPAS signal dependence on water vapor concentration for fixed CO concentrations. Using the procedure described in Section 4, QEPAS peak signal and absolute humidity were measured and are shown in Fig. 5. The theoretical calculations (Fig. 5a) have been compared with the corresponding results obtained at an integration time of 1*s*, for the CO concentrations of 0.5*ppm*, 0.75*ppm* and 1*ppm* in humidified-N_2 (Fig. 5b), as a function of the water vapor concentration. Experimental data were not acquired below the PTH detection range lower limit C_{Wb} (Fig. 5b). The theoretically predicted minimum in $\mathscr{H}_2(C_W)$ experimentally occurs in the QEPAS signal for a water vapor concentration of $C_{Wt} \sim 0.19\%$ for every CO concentration, thus proving that the endothermic to exothermic transition does not depend on CO concentration, as predicted in Section 3.1.

Another evidence of the endothermic to exothermic transition is given by the phase shift in the peak signal. In QEPAS technique, 2*f* signal phase on the absorption peak is related to the phase of the frequency-modulated source by the [9,22,26,27]:

$$tan\varphi_P = -2\pi\left(f_{QTF}/2\right)\tau_{rel} \quad (17)$$

where τ_{rel} represents the overall relaxation time.

To approximately predict phase shift $\Delta\varphi_P$, the following argument may be used. An ideal transition from an instantaneous endothermic relaxation to an instantaneous exothermic relaxation would lead to a $\Delta\varphi_P = 180°$ shift, for any pressure value.

Taking now into account the actual relaxation timescales in this experiment, the overall relaxation time τ_{rel} may be evaluated as [22,31]: $\tau_{dry} \approx (\gamma^{VV}_{CO-N2} \wp_{N2})^{-1} \approx 10.85\mu s$ for dry mixture and $\tau_{sat} \approx \left(\gamma^{VV}_{CO-H2O}\wp_{H2O} + \gamma^{VV}_{CO-N2}\wp_{N2}\right)^{-1} \approx 6.81\mu s$ for saturated mixture, leading to: $\varphi_{P,dry} \approx 23.05°$ *and* $\varphi_{P,sat} \approx (180° - 14.95°)$, giving a phase shift $\Delta\varphi_P = \varphi_{P,sat} - \varphi_{P,dry} \approx 142°$. As a term of comparison, for a gas pressure of 200*Torr* the related phase shift is smaller ($\Delta\varphi_P \approx 99.50°$), whereas at atmospheric pressure is greater ($\Delta\varphi_P \approx 154.40°$). In general, the slower is the relaxation process (which for fixed mixture components depends only on the number of collisional partners, i.e., on the gas pressure), the less evident becomes the phase transition.

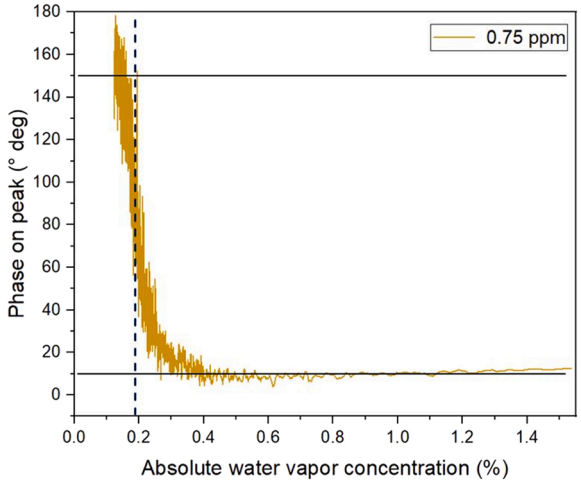

Fig. 6. Signal phase on QEPAS peak versus absolute water vapor concentration (retrieved via PTH), at a CO:N_2 concentration of 0.75 ppm. The vertical blue dashed line marks the C_{Wt} value (0.191%), horizontal black straight lines are guides for the eye marking 10° and 150° values.

In Fig. 6 the phase of the peak signal is plotted versus water vapor concentration, for a fixed CO concentration of 0.75*ppm*.

The measured phase shift $\Delta\varphi_P \approx 140°$, nearly matching the theoretical one, occurs at the threshold water humidity $C_{Wt} = 0.191\%$ (see the dashed blue line in Fig. 6), which corresponds to the inflection point, and physically represents the turnover between the two relaxational behaviors.

4.3. Water vapor-promoted CO relaxation in synthetic air

With the aim to investigate how the presence of an energy relaxation quencher as O_2 (see [12,13,21,22,29]) affects CO relaxation at atmospheric-like concentrations, measurements reported in Section 4.2 were repeated by replacing the diluting gas (N_2) with synthetic air

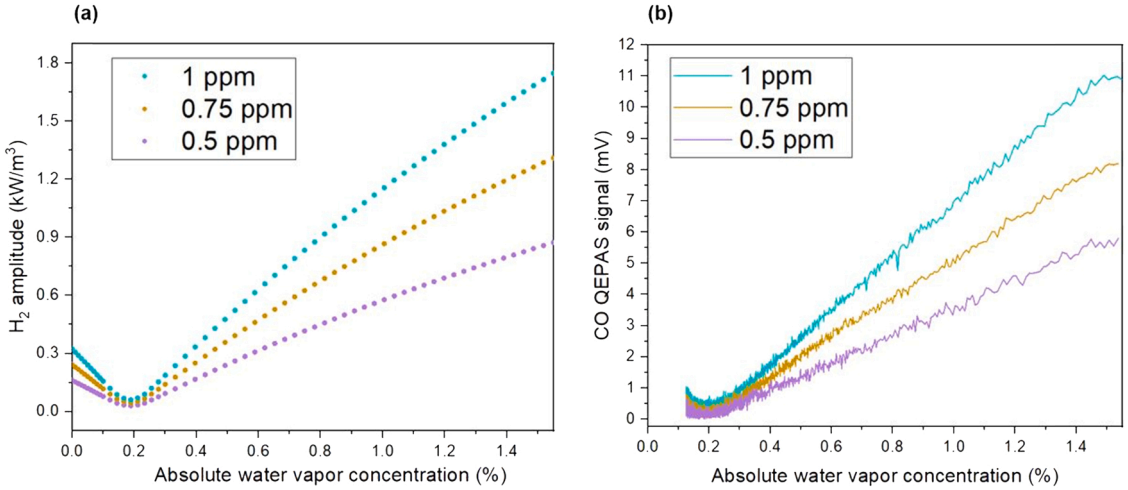

Fig. 5. a): theoretical calculation of the $\mathscr{H}_2$ for different values of CO concentration diluted in N_2. b): CO QEPAS peak signal versus absolute water vapor concentration. H_2O concentration values below $C_{Wb} = 0.125\%$ are not detectable with the employed PTH system.

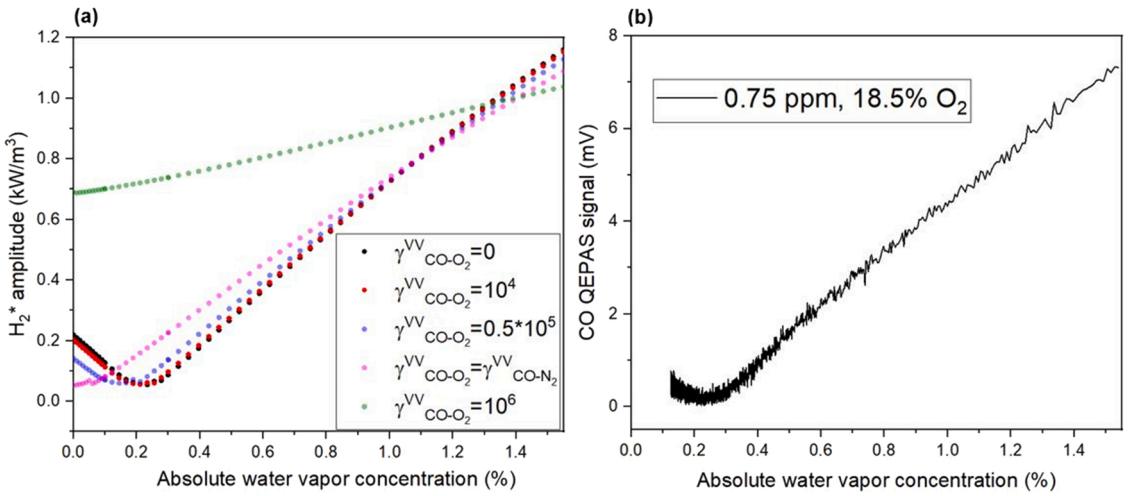

Fig. 7. a): simulations for $\mathscr{H}_2{}^*$ amplitude versus water vapor concentration for 750 ppb CO diluted in synthetic air, obtained for different values of γ^{VV}_{CO-O2}, all values of relaxation rates are expressed in $s^{-1}atm^{-1}$. b): measured QEPAS peak signal of 0.75 ppm of CO in synthetic air.

(certified $21\%O_2 : 79\%N_2$), for a CO concentration of 0.75*ppm*. The $\mathscr{H}_2{}^*(C_W)$ simulated curves, calculated for different values of the parameter γ^{VV}_{CO-O2}, are shown in Fig. 7a, while the CO QEPAS peak signal is plotted in Fig. 7b, both as a function of mixture humidity.

In Fig. 7b, the minimum in the QEPAS signal of CO in humidified synthetic air occurs at a water vapor concentration of $C'_{Wt} = 0.229\%$, greater than the concentration value $C_{Wt} = 0.191\%$ measured for CO in humidified nitrogen. Therefore, the obtained experimental results indicate that O_2 acts as a quencher in CO non-radiative de-excitation in the mid-IR spectral range, delaying the effect of water induced promotion and, thus, shifting the minimum of the QEPAS signal to higher values of humidity with respect to the case of CO diluted in N_2.

The comparison between the simulation and experimental results show that the hypothesis $\gamma^{VV}_{CO-O2} > 10^4 s^{-1}atm^{-1}$ must be rejected because either $\mathscr{H}_2{}^*(C_W)$ do not show any minimum (as for $\gamma^{VV}_{CO-O2} \geq \gamma^{VV}_{CO-N2}$ simulations, green and pink dotted curves in Fig. 7a), or the minimum occurs for lower values of water vapor concentration (blue dotted curve). It can therefore be stated that $\gamma^{VV}_{CO-O2} \leq 10^4 \quad s^{-1}atm^{-1}$.

In saturated humidity conditions, the presence of atmospheric O_2 reduces the QEPAS CO signal of ~11.5%. Therefore, to correctly convert QEPAS signals retrieved in saturated atmospheric air into actual CO concentrations, the calibration curve retrieved from Eq. (16) must be modified as:

$$S_{CO,sat,air} = 9.57(mV/ppm)C_{CO}(ppm) + 0.11mV \tag{18}$$

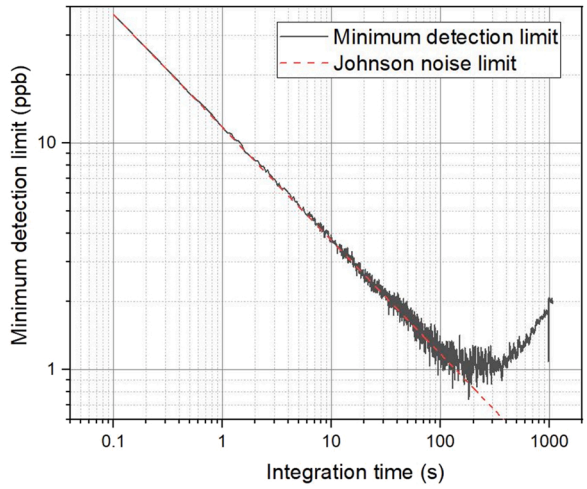

Fig. 8. Allan deviation analysis expressed in terms of an overnight 15 h-long noise level measurement (black solid line), compared with the Johnson noise (red dashed line).

4.4. Allan-Werle deviation analysis

An Allan-Werle deviation analysis was performed to analyze the sensor stability and predict how the sensitivity can be enhanced by employing greater integration times. With this aim, a 15 h-long overnight acquisition was performed, obtained running the QEPAS sensor and fixing the QCL emission wavelength at the selected CO absorption line, while flushing pure N_2. The Allan-Werle deviation plot is reported in Fig. 8.

As it can be observed, the Allan-Werle plot nicely resembles the Johnson noise trend, related to $1/\sqrt{t}$ thermal noise, for integration times up to 100 s, whereas the rise at longer integration time can be attributed to slow mechanical oscillations of the system [32]. The Allan-Werle deviation for 1*s* integration time is $\sigma_{1s} = 0.11mV$ (in agreement with the σ_{1s} reported in Section 4.1), which leads to a minimum detection limit of 12*ppb* in air, a value that is far below the carbon monoxide concentration in troposphere (see with Section 1).

4.5. Outdoor validation

Since the sensor was designed and realized for air quality monitoring purposes, for its first outdoor validation the prototype was set close to the traffic light between Via Amendola and Via Omodeo, in the city of Bari, Italy. The portable QEPAS sensor was equipped with a filled humidifier to maintain a stable and saturated water concentration of 1.55% during the whole measurement, which lasted almost 7*h*, from 11:45 to 18:15, on Tuesday 15th of June 2021.

The integrated PTH hygrometer (shown in the 3D draft in Fig. 2) was employed to measure water vapor concentration throughout the whole acquisition period. Measured water concentration was online converted in signal enhancement in order to retrieve the correct CO concentration, thereby including also small fluctuations or drifts due to ambient temperature variation (< 5%). The QEPAS signal was real-time converted into CO concentration using Eq. 18.

In Fig. 9, the detected CO concentration is compared with the daily averages collected the same day by two monitoring stations located in Via Caldarola (~1.5 km south-east from the selected traffic light) and in Corso Cavour (~2 km north-west) by the regional agency ARPA Puglia [33]. Corso Cavour is located in the city center and thereby higher CO

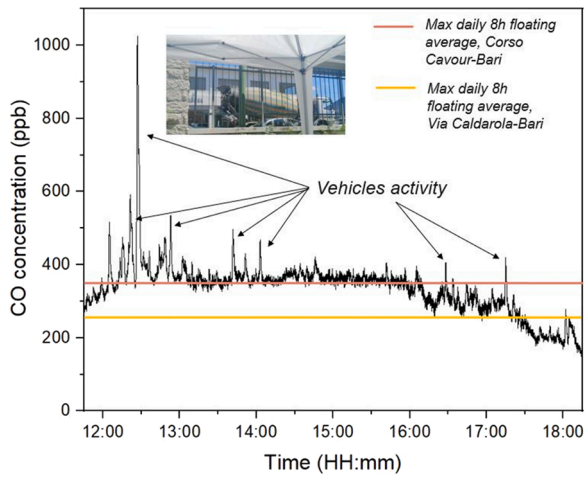

Fig. 9. CO concentration measured using the QEPAS prototype vs time, between 11:45 and 18:15, on Tuesday 15th of June 2021 near the traffic light between Via Amendola and Via Omodeo, in the city of Bari, Italy. The averaged CO levels for that day measured by ARPA Puglia in Bari on Corso Cavour (red straight line) and via Caldarola (yellow straight line) are also reported for comparison.

concentration values are expected.

The measured CO concentration values shown in Fig. 9 are consistent with the daily averages reported by ARPA Puglia on Tuesday 15th of June 2021. Values above the daily averages were recorded in the time span from 12:00 to 15:00, due to a high traffic congestion during to the lunch break for schools, universities and offices in surrounding area. CO concentration spikes corresponded to the passage of heavy-duty vehicles and, in particular, the highest one reported at 12:21 was measured during the passage of a concrete mixer, as documented by the photo in the inset of Fig. 9.

5. Conclusions

In this work, carbon monoxide non-radiative energy relaxation in the mid-IR spectral region has been investigated in a pure N_2 matrix and in an air-like gas matrix, by analyzing the QEPAS signal and phase behavior in terms of competing relaxational paths. A compact, rugged, and portable QEPAS-based CO sensor has been designed, realized, and calibrated in saturated humidity conditions. A minimum detection limit of 12*ppb* CO in air at 1*s* integration time was achieved. The prototype was employed to investigate the main CO energy relaxation processes in dry and humidified N_2 and in synthetic air matrixes. These studies allowed determining the upper limit ($\gamma^{VV}_{CO-O2} \leq 10^4 s^{-1} atm^{-1}$) for the relaxation rate related to the vibrational-to-vibrational collision $CO^* + O_2 \rightarrow CO + O_2{}^*$. Moreover, the calibration curve was corrected by taking into account the effect of oxygen in air as a quencher for CO energy relaxation in a humidified air matrix [31].

The sensor has been tested in-field to continuously monitor the carbon monoxide concentration in air close to a traffic light for seven hours. Measurements were performed in saturated humidity conditions, to reliably convert the QEPAS signal into CO concentration, employing the calibration curve. The retrieved CO concentration values were comparable with the daily averages reported by the local air inspection agency, thus proving the developed prototype as a reliable, fast response time sensor for highly sensitive real time CO detector.

Declaration of Competing Interest

The authors declare that there is no conflict of interest.

Acknowledgments

The authors from Dipartimento Interateneo di Fisica di Bari acknowledge funding from the European Union's Horizon 2020 Research and Innovation Program under grant agreement No. 101016956 PASSEPARTOUT, in the context of the Photonics Public Private Partnership and THORLABS GmbH within the PolySenSe joint-research laboratory. Dr. Marilena Giglio acknowledges POR PUGLIA FESR-FSE 2014 / 2020 – Asse X – Azione 10.4. Research for Innovation – REFIN.

References

[1] W.H.O. WHO, Air Quality Guidelines, Air Quality Guidelines. (2006) 1–496.
[2] V.I. Grover, Atmospheric Composition, Encyclopedia of Global Warming and Climate Change. (2012) 477. ⟨https://doi.org/10.4135/9781412963893.n49⟩.
[3] I.B. Belikov, C.A.M. Brenninkmeijer, N.F. Elansky, A.A. Ral'ko, Methane, carbon monoxide, and carbon dioxide concentrations measured in the atmospheric surface layer over continental Russia in the TROICA experiments, Izv. - Atmos. Ocean Phys. 42 (2006) 46–59, https://doi.org/10.1134/S000143380601004X.
[4] X. Zhang, J. Liu, H. Han, Y. Zhang, Z. Jiang, H. Wang, L. Meng, Y.C. Li, Y. Liu, Satellite-observed variations and trends in carbon monoxide over Asia and their sensitivities to biomass burning, Remote Sens. 12 (2020), https://doi.org/10.3390/rs12050830.
[5] R.K. Angatha, A. Mehar, Impact of traffic on carbon monoxide concentrations near urban road mid-blocks, J. Inst. Eng. Ser. A 101 (2020) 713–722, https://doi.org/10.1007/s40030-020-00464-2.
[6] M.D. Garba, M.S. Yunusa, Assessing gaseous pollutants and air quality in some areas of Kano metropolis, Kano, Nigeria, Environ. Impact III 1 (2016) 125–134, https://doi.org/10.2495/eid160121.
[7] R. James Barnard, J. Weber, Carbon monoxide: a hazard to fire fighters, Arch. Environ. Health 34 (1979) 255–257, https://doi.org/10.1080/00039896.1979.10667410.
[8] J. Hayden, B. Baumgartner, B. Lendl, Anomalous humidity dependence in photoacoustic spectroscopy of CO explained by kinetic cooling, Appl. Sci. 10 (2020), https://doi.org/10.3390/app10030843.
[9] P. Patimisco, G. Scamarcio, F.K. Tittel, V. Spagnolo, Quartz-enhanced photoacoustic spectroscopy: A review, Sensors 14 (2014) 6165–6206, https://doi.org/10.3390/s140406165.
[10] S. Qiao, Y. He, Y. Ma, Trace gas sensing based on single-quartz-enhanced photoacoustic–photothermal dual spectroscopy, Opt. Lett. 46 (10) (2021) 2449–2452, https://doi.org/10.1364/OL.423801.
[11] S. Qiao, Y. He, Y. Hu, Y. Ma, Z. Lang, Quartz-enhanced photoacoustic-photothermal spectroscopy for trace gas sensing, Opt. Express 29 (4) (2021) 5121–5127. https://doi.org/10.1364/OE.418256.
[12] Y. Ma, R. Lewicki, M. Razeghi, F.K. Tittel, QEPAS based ppb-level detection of CO and N_2O using a high power CW DFB-QCL, Opt. Express 21 (2013) 1008, https://doi.org/10.1364/oe.21.001008.
[13] Y. Ma, R. Lewicki, M. Razeghi, X. Yu, F.K. Tittel, Sensitive detection of CO and N2O using a high power CW 4.61 μm DFB-QCL based QEPAS sensor, In Proceedings of the 2013 Conference on Lasers and Electro-Optics, CLEO 2013. 21 (2013) 20224–20232. ⟨https://doi.org/10.1364/cleo_at.2013.jw2a.80⟩.
[14] J. Hayden, B. Baumgartner, J.P. Waclawek, B. Lendl, Mid-infrared sensing of CO at saturated absorption conditions using intracavity quartz-enhanced photoacoustic spectroscopy, Appl. Phys. B: Lasers Opt. 125 (2019) 1–11, https://doi.org/10.1007/s00340-019-7260-6.
[15] D. Pinto, H. Moser, J.P. Waclawek, S. Dello Russo, P. Patimisco, V. Spagnolo, B. Lendl, Parts-per-billion detection of carbon monoxide: A comparison between quartz-enhanced photoacoustic and photothermal spectroscopy, Photoacoustics 22 (2021), 100244, https://doi.org/10.1016/j.pacs.2021.100244.
[16] S. Qiao, Y. Ma, Y. He, P. Patimisco, A. Sampaolo, V. Spagnolo, Ppt level carbon monoxide detection based on light-induced thermoelastic spectroscopy exploring custom quartz tuning forks and a mid-infrared QCL, Opt. Express 29 (2021) 25100–25108.
[17] HITRAN on the Web, (n.d.). ⟨https://hitran.iao.ru/molecule/simlaunch?mol=5⟩ (accessed July 2, 2021).
[18] F. Sgobba, G. Menduni, S. Dello Russo, A. Sampaolo, P. Patimisco, M. Giglio, E. Ranieri, V.M.N. Passaro, F.K. Tittel, V. Spagnolo, Quartz-enhanced photoacoustic detection of ethane in the near-IR exploiting a highly performant spectrophone, Appl. Sci. 10 (2020) 1–11, https://doi.org/10.3390/app10072447.
[19] P. Patimisco, A. Sampaolo, M. Giglio, S. Dello Russo, V. Mackowiak, H. Rossmadl, A. Cable, F.K. Tittel, V. Spagnolo, Tuning forks with optimized geometries for quartz-enhanced photoacoustic spectroscopy, Opt. Express 27 (2019) 1401, https://doi.org/10.1364/oe.27.001401.
[20] S. Dello Russo, M. Giglio, A. Sampaolo, P. Patimisco, G. Menduni, H. Wu, L. Dong, V.M.N. Passaro, V. Spagnolo, Acoustic coupling between resonator tubes in quartz-enhanced photoacoustic spectrophones employing a large prong spacing tuning fork, Sensors 19 (2019), https://doi.org/10.3390/s19194109.
[21] N. Barreiro, A. Peuriot, G. Santiago, V. Slezak, Water-based enhancement of the resonant photoacoustic signal from methane-air samples excited at 3.3 μm, Appl. Phys. B: Lasers Opt. 108 (2012) 369–375, https://doi.org/10.1007/s00340-012-5018-5.

[22] S. Schilt, J.P. Besson, L. Thévenaz, Near-infrared laser photoacoustic detection of methane: the impact of molecular relaxation, Appl. Phys. B: Lasers Opt. 82 (2006) 319–329, https://doi.org/10.1007/s00340-005-2076-y.
[23] P.F. Zittel, D.E. Masturzo, Vibrational relaxation of H2O from 295 to 1020 K, J. Chem. Phys. 90 (1989) 977–989, https://doi.org/10.1063/1.456122.
[24] R.T.V. Kung, R.E. Center, High temperature vibrational relaxation of H2O by H 2O, He, Ar, and N2, J. Chem. Phys. 2187 (1975) 2187–2194, https://doi.org/10.1063/1.430786.
[25] M. Šimečková, D. Jacquemart, L.S. Rothman, R.R. Gamache, A. Goldman, Einstein A-coefficients and statistical weights for molecular absorption transitions in the HITRAN database, J. Quant. Spectrosc. Radiat. Transf. 98 (2006) 130–155, https://doi.org/10.1016/j.jqsrt.2005.07.003.
[26] J. Hodgkinson, R.P. Tatam, Optical gas sensing techniques: a review, 24 (2013) 43.
[27] J. Reid, D. Labrie, Second-harmonic detection with tunable diode lasers – comparison of experiment and theory, Appl. Phys. B Photo Laser Chem. 26 (1981) 203–210, https://doi.org/10.1007/BF00692448.
[28] J.D. Lambert, Vibrational and Rotational Relaxation in Gases, Clarendon Press, 1977.
[29] N. Barreiro, A. Vallespi, G. Santiago, V. Slezak, A. Peuriot, Influence of oxygen on the resonant photoacoustic signal from methane excited at the ν 3 mode, Appl. Phys. B: Lasers Opt. 104 (2011) 983–987, https://doi.org/10.1007/s00340-011- 4546-8.
[30] H.E. Bass, H.-J. Bauer, Kinetic model for thermal blooming in the atmosphere, Appl. Opt. 12 (1973) 1506, https://doi.org/10.1364/ao.12.001506.
[31] S. Dello Russo, A. Sampaolo, P. Patimisco, G. Menduni, M. Giglio, C. Hoelzl, V.M. N. Passaro, H. Wu, L. Dong, V. Spagnolo, Quartz-enhanced photoacoustic spectroscopy exploiting low-frequency tuning forks as a tool to measure the vibrational relaxation rate in gas species, Photoacoustics 21 (2021), 100227, https://doi.org/10.1016/j.pacs.2020.100227.
[32] M. Giglio, P. Patimisco, A. Sampaolo, G. Scamarcio, F.K. Tittel, V. Spagnolo, Allan deviation plot as a tool for quartz-enhanced photoacoustic sensors noise analysis, IEEE Trans. Ultrason., Ferroelectr. Freq. Control 63 (2016) 555–560, https://doi.org/10.1109/TUFFC.2015.2495013.
[33] ARPA Puglia - Qualità dell'aria Inq 2, (n.d.). ⟨http://old.arpa.puglia.it/web/guest/qariainq2 ⟩ (accessed July 2, 2021).

Fabrizio Sgobba received the M.S. degree (cum laude) in Physics in 2018. Since 2018, he is a Ph.D. student at the PolySenSe Lab, in the University of Bari. From March 2020 to March 2021 was visiting student in Thorlabs GmbH, Munich, Germany. His research activity is focused on the design and development of Quartz Enhanced Photoacoustic Spectroscopy-based gas sensors prototypes for industrial applications and on the study of gas relaxation in complex airlike matrices.

Angelo Sampaolo obtained his Master degree in Physics in 2013 and the Ph.D. Degree in Physics in 2017 from University of Bari. He was a visiting researcher in the Laser Science Group at Rice University from 2014 to 2016. Since March 2021, he is assistant professor at the Polytechnic of Bari. His research activity has included the study of the thermal properties of heterostructured devices via Raman spectroscopy. Most recently, his research interest has focused on the development of innovative techniques in trace gas sensing, based on Quartz-Enhanced Photoacoustic Spectroscopy, Tunable Laser Diode Absorption Spectroscopy, Light-Induced Thermoelastic Spectroscopy and covering the full spectral range from near-IR to THz. He is author of more than 100 Scopus publications and of more than 50 conference contributions. He is CEO and cofounder of PolySense Innovations.

Pietro Patimisco obtained the Master degree in Physics (cum laude) in 2009 and the Ph.D. Degree in Physics in 2013 from the University of Bari. Since 2020, he is Assistant professor at the University of Bari. He was a visiting scientist in the Laser Science Group at Rice University in 2013 and 2014. He is co-founder of PolySenSe Innovations. Dr. Patimisco's scientific activity addressed both micro-probe optical characterization of semiconductor optoelectronic devices and optoacoustic gas sensors. Recently, his research activities included the study and applications of trace-gas sensors, such as quartz enhanced photoacoustic spectroscopy and cavity enhanced absorption spectroscopy in the mid infrared and terahertz spectral region. He is author of more than 100 scientific papers published on international journals with impact factor and of more than 50 conference contributions, 6 as invited speaker.

Marilena Giglio received the M.S. degree (cum laude) in Applied Physics in 2014, and the Ph.D. Degree in Physics in 2018 from the University of Bari. In 2012 she's been visiting the Academic Medical Center of Amsterdam as a trainee. In 2015 she was a Research Assistant with the Department of Physics, University of Bari. She was a visiting researcher in the Laser Science Group at Rice University from 2016 to 2017. Since 2020, she is Assistant professor at the Physics Department of the Technical University of Bari. Her research activity is focused on the development of gas sensors based on Quartz-Enhanced Photoacoustic Spectroscopy and on the optical coupling of hollow-core waveguides with interband- and quantum-cascade lasers. She is author of more than 50 Scopus publications.

Giansergio Menduni received the M.S. degree (cum laude) in Electronic Engineering in 2017 and the Ph.D. degree in Electronic Engineering in 2021 from the Technical University of Bari. Since 2021, he is an assistant researcher at the Electric and Information Engineering Department of the Technical University of Bari. His research activity is focused on the development of gas sensors based on Quartz Enhanced Photoacoustic Spectroscopy and on the development of front-end electronics for piezoelectric sensitive elements.

Cristina Ranieri received the M.S. degree (cum laude) in Environmental Engineering in 2019 from the Polytechnic of Bari. Since 2019, she is a Ph.D. student in engineering for technological innovation at the Uninettuno University and at Physic Department of the Technical University of Bari. His research activity is focused on the application of gas sensors based on Quartz Enhanced Photoacoustic Spectroscopy.

Christine Hölzl received the Dipl.-Phys. and Dr. rer. nat. degrees from Technical University Munich in 2006 and 2012, respectively. During her Ph.D. thesis, her research interest was in the field of ultrafast optical orientation and time-resolved spectroscopy of carrier spin dynamics in semiconductor materials. Currently, she is contributing to the development of spectroscopy solutions at THORLABS GmbH.

Hubert Rossmadl obtained his Diploma degree in Physics in 2006 while working at the ASDEX-Upgrade Experiment from the Max-Planck Institute for Plasma Physics and the Ph.D. degree in Physics in 2013 from the Technical University of Munich. His research activity has included the study of solvated electrons with ultrafast time-resolved absorption and fluorescence- spectroscopy reached via non-linear optics. After two years of industrial production of frequency-converted single-mode lasers at Toptica, he is since 2016 at Thorlabs developing innovative compact sensors for trace gas detection based on Quartz Enhanced Photoacoustic Spectroscopy.

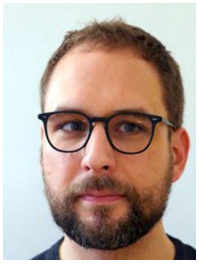

Christian Brehm received the diploma in Mechatronic Engineering in 2011 from the Friedrich- Alexander Universität Erlangen. In 2017, he joined Thorlabs Spectroscopy group. His research activity is focused on the development of gas sensors based on Quartz Enhanced Photoacoustic Spectroscopy and micro-assemblies of sensors.

Verena Mackowiak

Dario Assante received the Laurea degree and the Ph.D. in electrical engineering from the University of Naples Federico II. Actually he is Associate Professor at the International Telematic University Uninettuno. He has been the project manager of the Erasmus Strategic Partnership projects IN-CLOUD and IoT4SMEs, responsible for quality assurance of the Italo- Chinese satellite mission Limadou/CSES and academic referee of several Erasmus and LLP projects. His research interests are electromagnetic modeling, electromagnetic shielding, particle accelerators, energy efficiency and engineering education. He is author of more than 70 publications and 3 chapters in books.

Ezio Ranieri received the M.S. degree (cum laude) in Civil Engineering in 1990 from the University of Bari. Since 1994 he is Ph.D. in Environmental Engineering at the Polytechnic of Milan. He is Associate Professor at the University of Bari in Environmental and Sanitary Engineering. His research activity is focused on the environmental sensors monitoring.

Vincenzo Spagnolo obtained the Ph.D. in physics in 1994 from University of Bari. From 1997–1999, he was researcher of the National Institute of the Physics of Matter. Since 2004, he works at the Technical University of Bari, formerly as assistant and associate professor and now as full Professor of Physics. Starting from 2019, he become Vice-Rector of the technical university of Bari - Deputy to Technology Transfer. He is the director of the joint-research lab PolySense between Technical University of Bari and THORLABS GmbH, fellow member of SPIE and senior member of OSA. He is co-founder of PolySenSe Innovations. His research interests include optoacoustic gas sensing and spectroscopic techniques for real-time monitoring. His research activity is documented by more than 230 publications and 3 filed patents. He has given more than 50 invited presentations at international conferences and workshops.